Polymer Testing 101 (2021) 107313

Contents lists available at ScienceDirect

Polymer Testing

journal homepage: www.elsevier.com/locate/polytest

Strain induced crystallization in vulcanized natural rubber containing ground tire rubber particles with reinforcement and nucleation abilities

Nicolas Candau [a,*], Oguzhan Oguz [b,c], Carlos Eloy Federico [d], Gregory Stoclet [e], Jean-François Tahon [e], Maria Lluïsa Maspoch [a]

[a] Centre Català del Plàstic (CCP) - Universitat Politècnica de Catalunya Barcelona Tech (EEBE-UPC), Av. D'Eduard Maristany, 16, 08019, Spain
[b] Faculty of Engineering and Natural Sciences, Materials Science and Nano Engineering, Sabanci University, 34956, Orhanli, Turkey
[c] Sabanci University Integrated Manufacturing Technologies Research and Application Center, Composite Technologies Center of Excellence, Teknopark, Istanbul, Turkey
[d] Department of Materials Research and Technology (MRT), Luxembourg Institute of Science and Technology (LIST), ZAE Robert Steichen, L-4940, Hautcharage, Luxembourg
[e] Univ. Lille, CNRS, INRAE, Centrale Lille, UMR 8207 - UMET - Unité Matériaux et Transformations, F-59000, Lille, France

ARTICLE INFO

Keywords:
Wastes rubber
Natural rubber
Mechanical reinforcement
Strain induced crystallization

ABSTRACT

Strain induced crystallization (SIC) of peroxide vulcanized natural rubber (NR)/ground tire rubber (GTR) composites is studied by combining mechanical and microstructural characterization techniques. It is found that the incorporation of GTR into the NR matrix leads to more effective reinforcement at large strains at room temperature in the NR/GTR composites as compared to the neat NR. It is attributed to (i) the presence of the GTR particles acting as reinforcing fillers owing their high carbon black content, and (ii) the nucleating effect of the GTR for SIC in the NR matrix inducing further reinforcement through the generation of an increasing number of oriented crystallites that behave as supplementary reinforcing fillers.

1. Introduction

Recycling of waste rubber has received considerable attention in response to increasing demand for sustainable solutions for worldwide disposal problem of waste plastic/rubber [1,2]. Waste rubber can be recycled/reused as a high-added value additive in composite materials. This approach often leads to a significant enhancement in toughness of the matrix material in which waste rubber particles are incorporated [3–6]. However, it is a challenge to reintroduce waste rubber into the production cycle in the rubber industry as – in comparison to the fresh rubber – the added value it shows is limited, especially for to high waste contents (above 50 wt%).

Wastes rubber mostly originate from tires [7]. They typically contain vulcanized carbon black filled natural rubber (NR)/styrene butadiene rubber (SBR) compounds. For recycling purposes, end-life tires are first subjected to grinding (downsizing). The obtained ground tire rubber (GTR) is then devulcanized. The devulcanized GTR can then be incorporated into fresh rubber to design fresh/waste rubber composites. Mechanical properties of such materials depend on (i) the interfacial adhesion between the waste rubber particles and the fresh rubber matrix [8], (ii) the reduced size of waste rubber particles to improve the contact surface area with the fresh rubber matrix [9], and (iii) the extent of sulphur migration from the fresh matrix to the waste particles whose diffusion increases with decreasing particle size due to higher contact surface area [10].

Mechanical performance of the rubbery components in pneumatic tires, as well as in other natural rubber (NR) based composites, is related to their ability to undergo strain-induced crystallization (SIC) as reported by numerous reviews and book chapters [11–14]. In this regard, the effect of the vulcanizing system [15] and the network chain density [16] are two parameters of prime importance. Strain induced crystallization ability is not an exclusive property of natural rubber, and can be found in synthetic elastomers such as isoprene rubber (IR) [17], chloroprene rubber (CR) [18] or thermoplastic polyurethanes (TPU's) [19,20]. Nonetheless, SIC in NR is known to be more effective as compared to other synthetic elastomers [21]. This is mainly due to the high proportion of NR chains with cis 1,4 configuration (>98%) that facilitates their alignment upon deformation. SIC has also been studied in NR-based rubber composites such as natural rubber/isoprene (NR/IR) [22], NR/SBR [23], natural rubber/chloroprene (NR/CP) [24] and epoxidized NR/NR [25]. In addition, reinforcing fillers commonly incorporated into NR, such as carbon black fillers [26], silica [27],

* Corresponding author.
E-mail address: nico.candau@gmail.com (N. Candau).

https://doi.org/10.1016/j.polymertesting.2021.107313
Received 26 June 2021; Received in revised form 3 August 2021; Accepted 5 August 2021
Available online 8 August 2021

graphene oxides [28] or clay [29], are known to act as nucleating agents for promoting SIC in NR based composites.

Mechanical properties of NR based materials containing waste rubber have also been extensively investigated and tentatively ascribed to their ability to crystallize under strain. However, to the best of our knowledge, there is no direct evidence (e.g., observations by in-situ X-rays) for this phenomenon. On one hand, it has been shown that the incorporation of crystallizable wastes, such as waste Chloroprene rubber (CR) [30] or waste Latex [31], into NR enhances mechanical reinforcement of the resulting composites, attributed to their improved ability to crystallize under strain. On the other hand, it has been demonstrated that the addition of non-crystallizable waste rubber, such as nitrile butadiene rubber (NBR) [32], or ethylene propylene diene monomer (EPDM) [33], into NR generally shows a deterioration of the tensile strength, considered to be due to the decreased crystallizability of the materials.

Despite numerous investigations on the mechanical reinforcement in fresh/waste rubber composites, there is no direct demonstration of the occurrence of SIC in these materials. To address this issue, we focus in this paper on the mechanical reinforcement and strain induced crystallization in natural rubber/ground tire rubber (NR/GTR) composites, studied by applying a thermodynamic approach combined with mechanical response and in-situ X-ray scattering. This has enabled us to demonstrate that the large strain mechanical reinforcement in NR/GTR is mainly related to (i) the reinforcing effect of the waste GTR particles owing their high carbon black content, and (ii) their nucleating effect for SIC in the NR matrix inducing additional reinforcement through the formation of oriented strain-induced crystallites acting as new reinforcing fillers.

2. Materials and experiments

2.1. Materials and processing

The natural rubber (NR) is an SMR (Standard Malaysian Rubber) CV60 (Mooney Viscosity ML 1 + 4, 100 °C: 55–60), supplied by the company Akrochem (USA), with 0,15% of hydroxylamine added to the latex stage to prevent the raw rubber stiffening while storing. Ground tire rubber (GTR) was supplied by the company J. Allcock & Sons Ltd (United Kingdom) using the transformation of tire buffing into finer rubber crumbs via a controlled cryo-grinding. GTR is composed of 55 wt % of rubber (85 wt% of natural rubber, NR, and 15 wt% of Styrene Butadiene Rubber, SBR) and 45 wt% of carbon black (CB). The GTR crumbs are free of contaminants such as textile, metal and road dirt. The GTR particles were subsequently sieved using a vibratory sieve shaker (Analysette 3, Germany) with a mesh 120's (size <125 μm). Before processing, the GTR particles were dried overnight in a vacuum oven (Vaciotem-TV, J.P. SELECTA®, Spain) to prevent humidity absorption, over silica gel at 70 °C to remove any moisture. The natural rubber was masticated inside the chamber of an internal mixer (Brabender Plastic-Corder W50EHT, Brabender GmbH & Co., Germany) at a temperature of 80 °C, for 5 min and a rotation speed of 40 rpm. After 5 min of mastication, the GTR was added. After 5 more minutes the dicumyl peroxide (DCP) was added (1.5 wt% of the NR) as vulcanizing agent and mixed for 5 min. The obtained masterbatch containing NR, GTR and DCP was vulcanized according to the estimated optimal time at 170 °C [34] under 4 MPa.

2.2. Swelling

GTR was immersed in cyclohexane for 72 h and the solvent was changed every 24 h. After 72 h the swollen mass of (m_s) was measured. The GTR were then placed in an oven under vacuum at 70 °C during 6 h to remove the solvent. The mass of the dry samples (m_d) was then measured. The swelling ratio of the specimen Q and the network chain density were calculated from swelling and the Flory-Rehner equation [35]:

$$\upsilon = \frac{ln(1-v_2)+v_2+\chi_1 v_2^2}{V_1\left(-v_2^{\frac{1}{3}}+\frac{2}{f}v_2\right)} \quad (1)$$

with $v_2 = 1/Q_B$, $V_1 = 108\ cm^3/mol^{-1}$ is the molar volume of the solvent (cyclohexane), χ_1=0.353 is the Flory-Huggins natural rubber/cyclohexane dimensionless interaction term. One may note that χ_1 may change in presence of SBR contained in the GTR particles. The interaction parameters for vulcanized NR/SBR blends are indeed found to decrease linearly while increasing the SBR/NR content [36]. However, considering that SBR is only 15 wt% of the rubber included in the rubber phase of the GTR (see section 2.1), it gives a maximum SBR/NR ratio of 0.033 obtained for our NR/GTR33 blends. Hence, in this study we will consider the Flory-Huggins polymer solvent interaction term of the natural rubber/cyclohexane system.

The expression of the Flory-Rehner equation (Equation (1)) assumes the affine deformation which states that the deformation applied to cross-link positions is the same than the macroscopic deformation. The crosslink functionality, f, was chosen equal to 4, as initially proposed by Flory and Rehner [35]. The Kraus correction [37] was used to account for the contribution of filler in swelling ratio calculation, assuming that they do not contribute to swelling. Q_c is the swelling ratio of the rubber matrix defined as follows:

$$Q_c = \frac{Q-\phi}{1-\phi} \quad (2)$$

with ϕ is the volume fraction of fillers. Krauss correction in Equation (2) assumes non-adhesion of the fillers to the rubbery matrix in the swollen state. More detailed explanations on the procedure can be found in Refs. [38,39].

2.3. Scanning electron microscopy (SEM)

The fracture surfaces of the specimens were observed with a field emission scanning electron microscope (JSL-7001F, JEOL, Japan). A few nanometers thick conductive layer of a Pt80/Pd20 alloy was sputtered on the fracture surface using a high-resolution sputter coater (Cressington 208HR) in order to avoid electron charging. The surface topography was observed with a voltage of 1 kV. Chemical analysis was performed by EDX with a voltage of 20 kV.

2.4. Uniaxial tensile stretching (UTS)

Dogbone shaped specimens of type 1BA were extracted from hot moulded sheets by die-cutting with a specimen preparation punching machine (CEAST). The specimens have the following dimensions: 1 mm thickness, 5 mm width and 40 mm length. Uniaxial tensile tests according to the ISO 527 standard were performed on a universal testing machine (SUN 2500, GALDABINI) at room temperature and a constant crosshead speed of 100 mm/min. The machine is equipped with a video extensometer (OS-65D CCD, Minstron).

2.5. Micro-computed X-ray tomography (μCT)

3D morphological information of GTR was obtained by micro-computed X-ray tomography (μCT) carried out by a RX Solutions EasyTom 160 scanner using a tungsten filament. An acceleration voltage of 40 kV at a current of 80 μA were employed with a frame rate of 1.5 while averaging 5 frames per projection. A full rotation (360°) was used with projections taken every 0.25°. The source-to-object-distance (SOD) and source-to-detector-distance (SDD) were set for obtaining a voxel size of 2 μm. The 3D volume reconstruction of the projections was generated by the software Xact64. Image treatment and analysis were performed with the commercial software Avizo (Thermo Fisher Scientific). Inherent

noise of the acquired images was reduced by means of a median filter. Then, images were binarized by thresholding the grayscale histogram. A watershed algorithm was used for separating close objects. Next, elements represented by less than 3 voxels were removed for decreasing uncertainties due to their limited geometrical representation. This procedure enabled a spatial resolution of 7 μm, corresponding to the smallest object detected with accuracy. Finally, the binarized objects were characterized by their equivalent diameter (D_{eq}) defined as [40]:

$$D_{eq} = \sqrt[3]{\frac{6V}{\pi}} \tag{3}$$

2.6. Wide angle X-rays (WAXS)

A miniature tensile test machine was used to record 2D-WAXS patterns from specimens subjected to tensile strains. Tensile test-bars with a 0.5 × 4 mm^2 rectangular cross-section and 5 mm gauge length were prepared. The experiments were carried out owing to a Xeuss 2.0 apparatus (Xenocs) and the two-dimensional X-Rays scattering patterns are recorded by a Pilatus 200k hybrid pixel detector (Dectris) with a specimen-detector distance of 140 mm. The experiments are performed in transmission mode with a beam size of 500 μm × 500 μm. The exposure time is equal to 30 s. The intensity I_d due to air scattering and direct beam were measured in absence of any sample. They were removed from the total measured intensity scattered in the presence of the material I_{meas}. The corrected scattering intensity I_{corr} is written: $I_{corr} = I_{meas} - TI_d$ with T the transmission factor is equal to $e^{-\mu e}$, μ is the coefficient of transmission and e the thickness of the specimen is equal to $\frac{e_0}{\lambda}$ with λ the stretching ratio. Each scattering pattern was integrated azimuthally. The deconvolution of the curve $I = f(2\theta)$ enabled the extraction of the intensity at the peak top and the width at half height of each crystalline peak and the intensity at the peak top of the amorphous phase. The crystallinity index CI was then determined as follows:

$$CI = \frac{I_c}{I_a + I_c} \tag{4}$$

where I_c and I_a are the intensity of the crystalline and amorphous peaks respectively. The average crystallite sizes L_{hkl} in the direction normal to the (*hkl*) planes were estimated from the Scherrer equation:

$$L_{hkl} = \frac{K\lambda_w}{\beta_{1/2} cos\theta} \tag{5}$$

where $\lambda_w = 1.542$ Å is the X-ray wavelength and θ is the radial angle. In this study, each crystalline peak was fitted with a Lorentzian function for which the width at half-height is $\beta_{1/2}$. According to the parameters chosen for the fit of the experimental peak, K = 0.64.

3. Results and discussion

3.1. GTR particle distribution in the NR/GTR composites

Sieved GTR particles (Fig. 1a), containing traces of micron sized talc (Mg SEM-EDX signal) used for GTR grinding, were blended with natural rubber (NR) and peroxide vulcanized. The 2D representative tomography images of the resulting NR/GTR composites (Fig. 1b) show particles of different intensity in grey, which is directly related to the density of the phase. The white zones are the heavy particles of talc but also likely some traces of zinc oxide originating from the sulphur vulcanization of the tire. The grey particles correspond to the GTR. Their 3D rendering is depicted in representative volumes (Fig. 1c). Quantitative observations reveal the distribution of the GTR to be homogeneous in the analyzed volume (Fig. 1d). The homogeneous distribution of the GTR particles renders a shorter inter particle distance between them with increasing GTR content (Fig. 1d). The distance between the GTR particles will certainly impact the strain field during uniaxial deformation of the specimens and by inference influence their large strain mechanical reinforcement as will be discussed in the following.

3.2. Mechanical reinforcement in NR/GTR composites

Vulcanized NR and NR/GTR show a typical hyper-elasticity with a notable reinforcement at large strain at room temperature (Fig. 2a–d). In the frame of the gaussian approximation, the decreased in entropy upon stretching results in an elastic force written as follows [41]:

$$\sigma_g = \nu RT \frac{\langle r^2 \rangle}{\langle r_0^2 \rangle} \left(\lambda_c - \frac{1}{\lambda_c^2} \right) \tag{6}$$

where ν is the network chains density (in $mol.cm^{-3}$), $R = 8.314$ J K^{-1} mol^{-1}, is the gas constant, T the temperature (in K), and $\lambda_c = 1 + \varepsilon$ the strain in the composite. r is the end-to-end distance of the network chains (chain sequences extending from one cross-link to another), $\langle r_0^2 \rangle$ and $\langle r^2 \rangle$ represent the dimensions of the free chains in the unstretched and stretched states respectively. A simplified form of equation (6) [42]

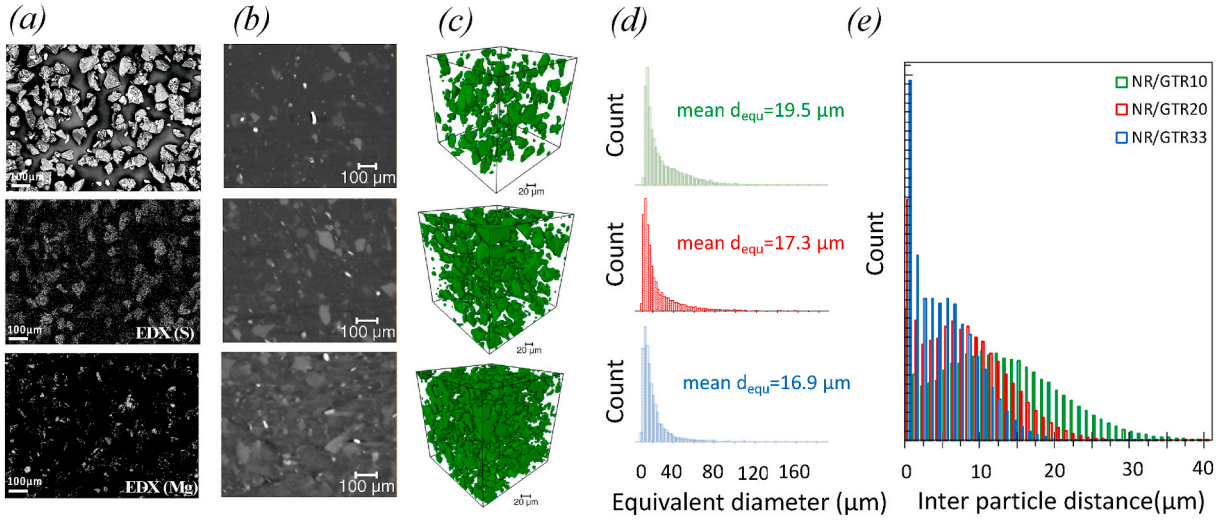

Fig. 1. *(a)* SEM (top) and SEM-EDX of GTR particles with elemental analysis (sulphur, center) and (Magnesium, bottom). *(b)* 2D and *(c)* 3D representative tomography images of the NR/GTR composites (from top to bottom: NR/GTR10, NR/GTR20, NR/GTR33). *(d)* Equivalent diameter distribution and *(e)* inter particles distances in the same NR/GTR.

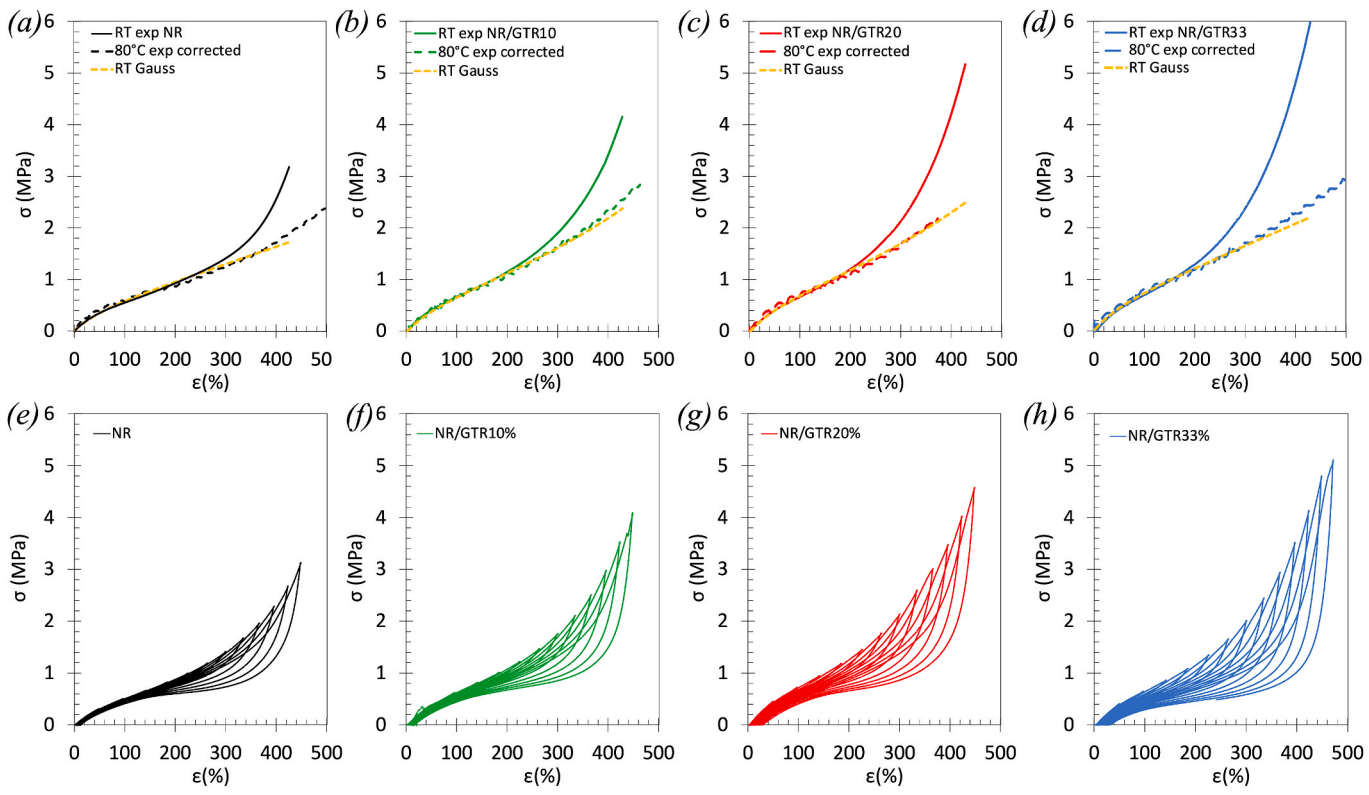

Fig. 2. *(a-d)* room temperature (solid lines), 80 °C (corrected from entropic effect) stress-strain curves of NR and NR/GTR composites. The dotted lines are fits from Gaussian behaviour (see equation (7)). *(e-h)* Tensile tests with incremental strain in the same materials.

assumes $\langle r^2 \rangle$ to be identical to $\langle r_0^2 \rangle$, which means that the cross-links do not significantly change the chain dimensions from their unperturbed values, and hence the expression of the stress from gaussian approximation can be written:

$$\sigma_g = \frac{E_c}{3}\left(\lambda_c - \frac{1}{\lambda_c^{\,2}}\right) \tag{7}$$

with $E_c = 3\nu RT$ which provides the relation between the crosslink density of the rubber chains and the elastic modulus of the composite.

The gaussian approximation is found to fit the experimental stress-strain curves up to a strain around 200%. One may note that the gaussian distribution of the end-to-end distance *r* is generally not a good approximation for filled rubbers. Indeed, the adsorption of polymer chains onto filler particles changes the mean value and the distribution of end-to-end vectors of the chains [43]. Nonetheless, low filler content is expected to result in moderate modification of both the mean value and distribution of *r*. In our materials, the quantity of carbon black is assumed sufficiently low (2.1, 4.3 and 7.5 vol% for NR/GTR10, NR/GTR20 and NR/GTR33 respectively) so that the deviation from the gaussian approximation used for unfilled rubber is expected to not be meaningful.

At higher strains (>200%), stress strain curves diverge. Interestingly, the divergence is even more pronounced in the NR/GTR composites, providing a clear-cut evidence for a non-gaussian reinforcement in the specimen at room temperature. It is known that such reinforcement results from the strain-induced crystallization in vulcanized NR [14]. However, to the best of our knowledge, it has not yet been demonstrated in the case of NR/wastes rubber blends. In contrast, at 80 °C, the materials do not show reinforcement anymore. The assumption of a purely entropic elasticity for these high temperature tests, as predicted by equation (6), suggests the stress to be directly proportional to the absolute temperature. One can refer for instance to the dedicated study by Mark [44]. Hence, we corrected from the temperature dependence of the entropic elasticity (correction factor on the stress of (21 + 273)/(80 + 273)), and the stress strain curves were found to follow the room temperature gaussian behaviour, suggesting that the non-gaussian reinforcement, likely due to SIC, is suppressed at this temperature in the strain range studied. It should be noted that, in spite of the suppression of SIC at high temperature, a slight reinforcement is observed by increasing GTR, suggesting that the GTR act as reinforcing filler (without influencing the SIC) due to their high carbon black content (∼ 45 wt%). This is consistent with other studies showing that the GTR particles can cause a mechanical reinforcement, even in non-crystallizable rubber composites such as SBR/GTR [45]. To corroborate the occurrence of SIC in NR/GTR, we performed incremental cyclic tests under tension (Fig. 2e–h). The observed dissipated energy in NR and NR/GTR composites is likely caused by the "super-straining" effect due to the difference in strain at crystallization and strain at melting [46].

One may note that cavitation is known to compete with strain induced crystallization in filled natural rubber [27,47]. However, this phenomenon is expected to be less predominant in our NR/GTR blends as compared to industrial filled elastomers [48,49] due to the reasonable amount of carbon black, i.e. 2.1; 4.3, 7.5 vol% in the case of NR/GTR10, NR/GTR20 and NR/GTR33 respectively. This is consistent with the rather low permanent strain observed during the incremental tests as compared to industrial filled elastomers. Nonetheless, decohesion/cavitation at NR/GTR interface may possibly occur, that could be solved by further in-situ SAXS and μCT studies.

To highlight the deviation from the gaussian behaviour, we calculated the difference in mechanical energy (energy gap) required for the deformation of gaussian chains and the experimental deformation energy. This energy difference is written as follows:

$$W_{gap}(\lambda) = \int_1^{\lambda} (\sigma_{exp} - \sigma_g)\, d\lambda \tag{8}$$

The deformation energy was obtained from the integral of the stress-strain curves (area under the experimental stress-strain curve) and the deformation energy associated with gaussian approximation:

$$W_{gap}(\lambda) = -\frac{E_c}{6}\left({\lambda_c}^2 + \frac{2}{\lambda_c} - 3\right) + \int_1^{\lambda} \sigma_{exp} d\lambda \quad (9)$$

The plot of the difference in mechanical energy between the gaussian approximation and the experimental tensile curve evidences a decreased strain at the onset of non-gaussian reinforcement while increasing the GTR content (Fig. 3a). In addition, the energy dissipation obtained from incremental tests plotted as a function of the strain (Fig. 3b) confirms an early occurrence of SIC with strain while increasing the GTR content.

3.3. Local entropy changes at the origin of the reinforcement

As previously mentioned from the observation of μCT images, GTR particles may increase the local strain field in the NR matrix that can be estimated by applying a simple thermodynamic approach (Fig. 4, equations (10) and (11)). A strain amplification in NR/GTR composites is assumed to arise from the weak deformability of the GTR particles as compared to the NR matrix due to the non-negligible content of non-deformable CB particles (~ 45 wt%). A strain amplification factor, A, deduced from the Guth and Gold equation [50] is used to describe the local strain in the rubber chains of the NR matrix that accounts for the presence of the undeformable CB particles in the GTR particles:

$$A = \frac{\lambda_{r,i} - 1}{\lambda_{c,i} - 1} = 1 + 2.5\phi + 14\phi^2 \quad (10)$$

with $\lambda_{c,i}$ the strain at reinforcement onset of the composite, as measured experimentally from the deviation of the stress-strain curve from the room temperature gaussian behaviour (see Fig. 3a), $\lambda_{r,i}$ is the local strain of the NR matrix at reinforcement onset that, expectedly, is found to increase with GTR content (Fig. 4a). The configurational entropy of the rubber chains is a driven factor for SIC [51]. The decrease in local chain entropy at the strain onset of reinforcement is given by the integration of equation (7) to give:

$$\Delta S_{r,i} = -\frac{\nu_{r,g} R}{2}\left({\lambda_{r,i}}^2 + \frac{2}{\lambda_{r,i}} - 3\right) \quad (11)$$

The network chain density of rubber chains, ν_{rs}, estimated from swelling (equations (1) and (2)) is found to be around 1.1×10^{-4} mol cm^{-3} for the blends with GTR contents up to 20 wt% and then decreases (Fig. 4b). One may note that ν_{rs} in the neat NR is found to be very close to the one of the individual GTR particles (1.0×10^{-4} mol cm^{-3}) as determined in Ref. [6], suggesting the network chain density in the NR/GTR composite to be representative of the one in the NR matrix. Interestingly, ν_{rs} estimated from swelling, shifted to a value of 0.5×10^{-4} mol cm^{-3} (the shift may account for entanglement contribution) coincides relatively well with the one estimated from gaussian approximation. The resulting entropy changes in the NR matrix at the strain onset of mechanical reinforcement (equation (11)) is found to slightly increase with increasing GTR content (Fig. 4c). Possible uncertainties in entropy changes may arise from rubber chains network heterogeneities [15], not taken into account in the present approach. Moreover, the increase of neighbor GTR particles in the composites (Fig. 1e) may result in additional stress concentration favorable to SIC, like in the case of carbon black filled vulcanized NR [52]. Nonetheless, it should be noted that the variations in local entropy change with the GTR content are weak, in contrast to the trend observed in sulphur cured NR [53], suggesting this thermodynamic parameter to satisfactorily predict the initiation of mechanical reinforcement in both NR and NR/GTR composites.

3.4. X-rays observation of strain-induced crystallization in NR/GTR composites

In the previous sections, we have demonstrated that room temperature mechanical reinforcement in NR/GTR composites is *a priori* related to the occurrence of strain induced crystallization in the NR matrix and governed by the decreased entropy of the natural rubber chains. Here, we aim to investigate SIC in these materials by in situ WAXS to obtain quantitative data on the crystal structure, such as the evolution with strain of the crystalline volume fraction, the volume, number and orientation of the crystallites. (Figs. 5–8). The 2D scattering patterns obtained at different specimen deformation (Fig. 5) clearly show the transformation from an initially isotropic amorphous state to an anisotropic semi-crystalline state as evidenced by the appearance of the crystalline plane reflections (002), (200), (120) and (210) typical from monoclinic crystal structure [54] with the c axis parallel to chains axis and oriented in the tensile direction.

The WAXS crystallinity index (equation (4)), reveals that SIC appears at a deformation around 300% for the vulcanized NR (Fig. 6a), and the maximum crystallinity index measured at a deformation around 570% is around 8 vol%. Such behaviour is consistent with what is observed for peroxide cured NR with a similar network chains density [53].

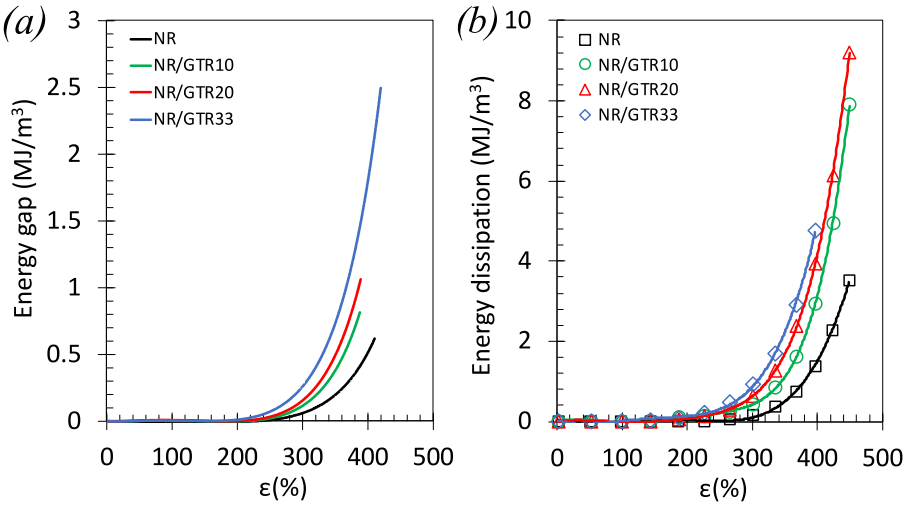

Fig. 3. (a) Difference of strain energy (energy gap) between the experimental stress-strain curve and the gaussian approximation obtained from equation (9), and (b) energy dissipation obtained from tensile cycles with incremental strain obtained from Fig. 2e–h.

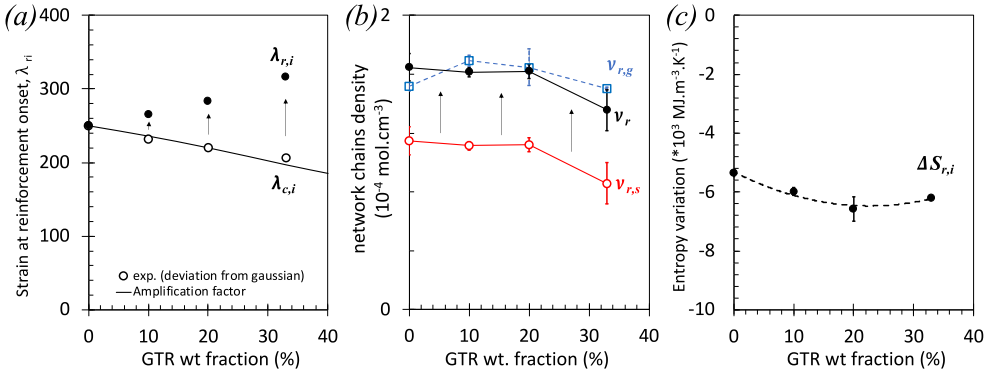

Fig. 4. *(a)* Strain onset of mechanical reinforcement estimated from deviation from gaussian behaviour (see Fig. 3a) assuming a rise of 0.01 MJ m^{-3} to be characteristic of the deviation onset (unfilled ring symbols), and local strain onset of mechanical reinforcement estimated from equation (10) (filled ring symbols). *(b)* Network chain density in the NR matrix estimated from the gaussian approximation, $\nu_{r,g}$, from swelling, $\nu_{r,s}$, and from swelling shifted to + 0.5 × 10^{-4} mol cm^{-3}, ν_r. *(c)* Entropy variation at strain onset of reinforcement versus the GTR content. The value of network chains density may be expressed in mol.m^{-3} by multiplying the value in Fig. 4b by a factor 100.

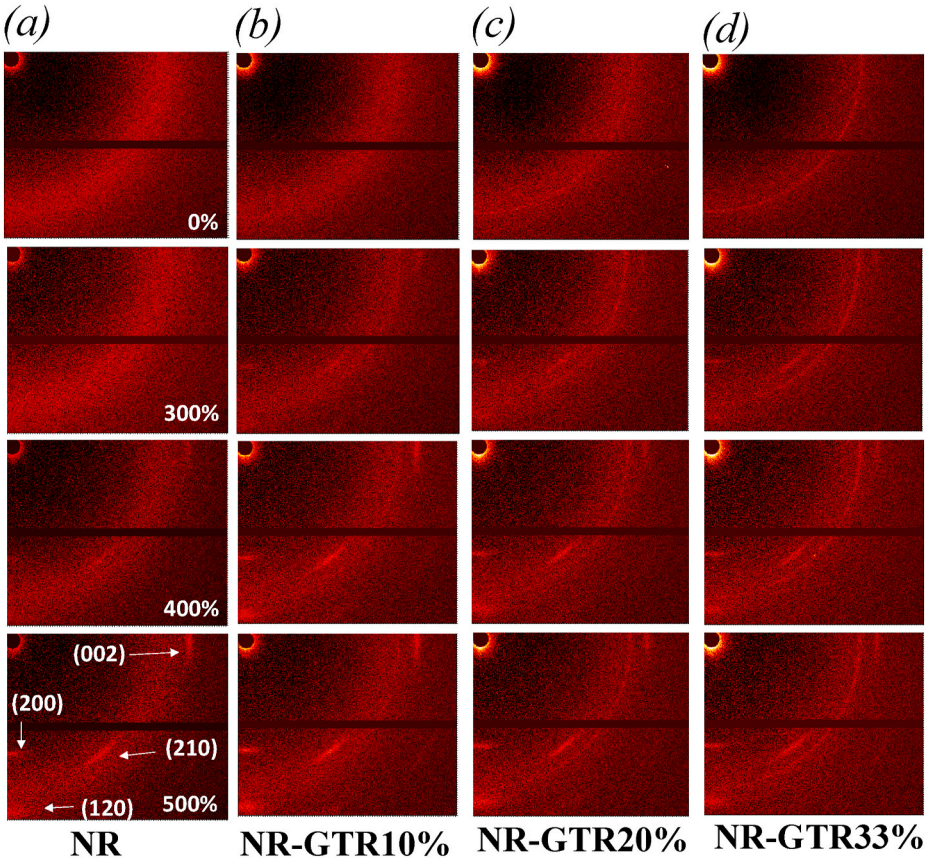

Fig. 5. 2D WAXS patterns of the NR and NR-GTR blends at different deformations from 0% to 500% (from top to bottom) for *(a)* NR, *(b)* NR/GTR10, *(c)* NR/GTR20 and *(d)* NR/GTR33. The patterns are shown after subtraction of the direct beam.

Interestingly, SIC is found to appear at a lower strain in the NR/GTR composites, consistent with above observations based on mechanical approaches using the deviation from gaussian approximation (Fig. 3a) and the dissipated energy (Fig. 3b). This demonstrates a nucleation ability of the GTR particles on SIC in NR, associated with a faster increase of crystalline phase in the NR/GTR10 and NR/GTR20 with strain. It results, in the final stages of the tensile test, in an optimum crystallinity index for these two materials. As evidenced by a more limited ability of the NR/GTR33 to crystallize at highest strain, an exceedingly high amount of GTR may tend to limit the NR crystallizability. While the decreasing GTR inter particle distance (Fig. 1e) may initially contribute to a strain localization and by inference favors the occurrence of SIC, a further development of SIC at larger strain is slowed down, that can arise from a decreasing nucleation and/or crystal growth rates.

An analysis of the size, number, and orientation of the SIC crystals (Figs. 7–8) is aimed to provide further information on the nucleation/growth process of SIC in NR/GTR composites. The crystallite size in the direction normal to the planes (120), (002) and (200), namely the lengths L_{120}, L_{002} and L_{200}, respectively, show a regular decrease and then stabilization with applied deformation. Such trend is observed for both the NR and the NR/GTR composites. Slight decrease of the dimension of the crystallites with increasing GTR content is observed as compared to the neat NR, similar to what has been reported for CB filled NR [26,55]. In the case of NR/GTR blends, the initially microscopic GTR inter particle distance (Fig. 1e) may sufficiently decrease with strain to induce a confinement of the crystallizable NR domains in the inter particle regions that may result in a limitation of the lateral crystallites growth.

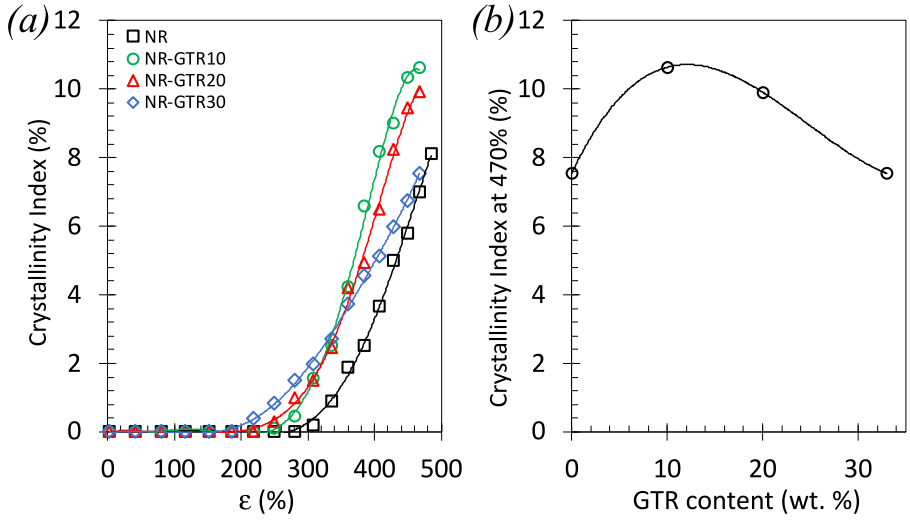

Fig. 6. *(a)* WAXS crystallinity index (equation (4)) versus the strain for the different NR/GTR composites and *(b)* the crystallinity index at the strain of 470% as a function of the GTR wt. fraction in the NR/GTR composites.

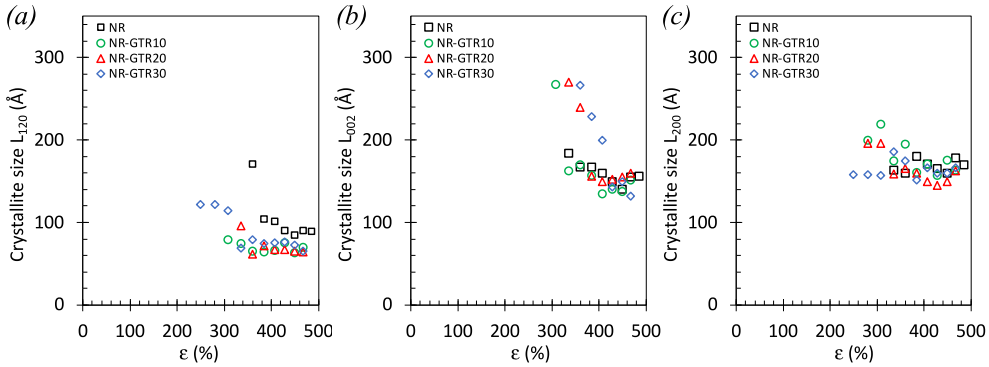

Fig. 7. *(a)* Crystallite size L_{120}, *(b)* crystallite size L_{002}, and *(c)* crystallite size L_{200}, of NR (black square symbols), NR/GTR10 (green ring symbols), NR/GTR20 (red triangle symbols) and NR/GTR33 (blue diamond symbols). (For interpretation of the references to colour in this figure legend, the reader is referred to the Web version of this article.)

The measures of three principal planes of the crystals has enabled us to estimate the average volume of the crystallites, that is given by Ref. [46]:

$$V_c = 0.94 L_{200} L_{120} L_{002} \tag{12}$$

From equation (12), the average number of the crystallites per unit volume N is written:

$$N = CI / V_c \tag{13}$$

One may note that this average number, N, is only qualitative. Hence, it is estimated from the crystallinity index, CI, that does not necessarily reflect the absolute volume fraction of the crystalline phase. A recent work of Le Cam demonstrated that the WAXS crystallinity index and the crystalline fraction obtained from infrared measures fit well [56], however IR thermography also shows some limitation, such as the fact that a measure of the traces of heat at the specimen surface may not fully reflect the true heating due to strain induced crystallization in the specimen volume. A direct comparison of DSC crystalline fraction and WAXS crystallinity index is still missing in the literature and would be relevant to clearly discuss on the validity of each experimental method (WAXS, IR or DSC) to determine the true crystalline fraction. In this study, the WAXS crystallinity index, CI, and hence, the crystallites number deduced from it, N, is used as a relative value for sake of comparison between materials.

The crystallites volume is found to widely decrease with the deformation for both NR and NR/GTR composites and reach a minimum at highest strain (Fig. 8a). The final volume of crystallites in NR/GTR is found to be lower than that of the NR. From equation (10), the crystallites number is found to almost linearly increase with the applied deformation, more rapidly in NR/GTR composites as compared to NR (Fig. 8b). This suggests that the presence of GTR particles in the NR matrix favors the multiplication of strain induced crystallites, confirming their nucleation ability not only at the incipient strain as previously discussed (Fig. 4b), but also at higher strains, with the highest nucleation rate for the NR/GTR10 and NR/GTR20. Interestingly, the orientation of crystals estimated from the azimuthal distribution of the normal to the planes (200) is found to not be limited by the presence of the GTR particles (Fig. 8c). This is in contrast with mechanisms observed in carbon black filled NR where crystals orientation is significantly restricted [26,53]. The ability of the NR matrix to maintain the anisotropy of the SIC crystals in the NR/GTR composites may contribute to the mechanical reinforcement; these oriented SIC crystals acting as new reinforcing fillers.

4. Conclusion

We demonstrated the occurrence of strain induced crystallization (SIC) in peroxide vulcanized Natural Rubber (NR)/Ground Tire Rubber

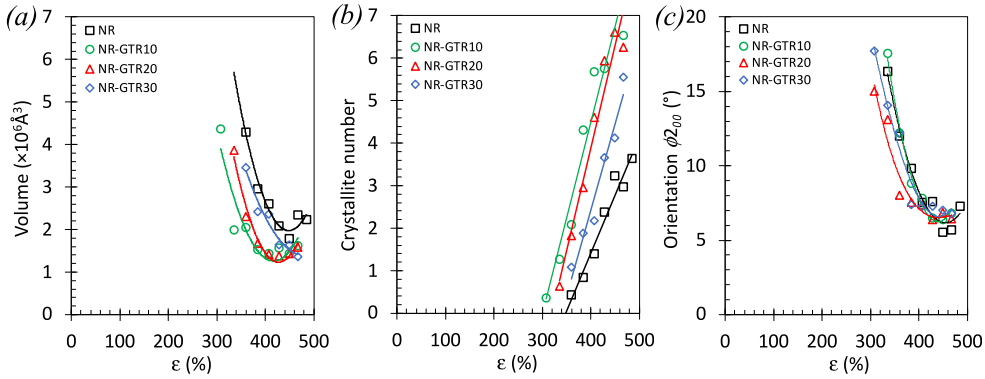

Fig. 8. *(a)* Volume of the crystallites, *(b)* crystallites number and *(c)* crystallite orientation Φ_{200} of the NR and the NR/GTR composites as a function of the applied deformation.

(GTR) composites by using in situ X-Rays radiation during their uniaxial deformation. The strain at crystallization onset was found to regularly decrease by increasing the GTR content and the fraction of the crystalline phase in the NR matrix was found to increase with an optimum of 10–20 wt% of GTR. This behaviour was ascribed to the role of GTR as nucleating agents for SIC through an increase of the local strain in the NR matrix. This has been supported by a simple thermodynamic approach accounting for the strain amplification arising from the presence of undeformable carbon black particles in the GTR.

The improved SIC was accompanied by a more rapid orientation of the crystallites as well as a higher number of highly oriented crystallites with increasing strain. The latter act as new crystalline fillers which, in addition to the intrinsic reinforcing effect of the GTR particles, promotes the large strain reinforcement in the NR/GTR composites.

The observation and in-depth characterization of SIC in wastes GTR filled NR based composites is considered to be of significance for industrial applications in which the main goal is to achieve not only the large strain mechanical reinforcement, but also the fatigue resistance and/or the giant elastocaloric effect with the reuse of wastes particles as high-added value additives, with the further ambition to participate in the development of sustainable solutions for worldwide wastes disposal problem. Moreover, the improvement of wastes treatment, such like the use of wastes rubber particles devulcanization, may be beneficial to improve the reinforcement and strain induced crystallization properties of the resulting NR/GTR blends by improving the strength at NR/GTR interface.

Authorship contributions

Conception and design of study: Nicolas Candau. Acquisition of data: Nicolas Candau, Carlos Eloy Federico, Gregory Stoclet, Jean-François Tahon. Analysis and/or interpretation of data: Nicolas Candau, Oguzhan Oguz, Carlos Eloy Federico, Gregory Stoclet. Drafting the manuscript: Nicolas Candau, Oguzhan Oguz, Maria Lluïsa Maspoch. Revising the manuscript critically for important intellectual content: Nicolas Candau. Approval of the version of the manuscript to be published: Nicolas Candau, Oguzhan Oguz, Carlos Eloy Federico, Gregory Stoclet, Jean-François Tahon, Maria Lluïsa Maspoch.

Declaration of competing interest

The authors declare that they have no known competing financial interests or personal relationships that could have appeared to influence the work reported in this paper.

Acknowledgements

The research leading to these results has received funding from the European Union's Horizon 2020 research and innovation programme under the Marie Skłodowska-Curie grant agreement No 712949 (TECNIOspring PLUS) and from the Agency for Business Competitiveness of the Government of Catalonia. The project ARCHI-CM, Chevreuil Institute (FR 2638), Ministère de l'Enseignement Supérieur et de la Recherche, Région Nord-Pas de Calais and European Regional Development Fund (FEDER) are acknowledged for supporting and funding the SAXS-WAXS laboratory equipment.

References

[1] European Commission, A European Strategy for Plastics in a Circular Economy, 2018.
[2] M. Sienkiewicz, H. Janik, K. Borzędowska-Labuda, J. Kucińska-Lipka, Environmentally friendly polymer-rubber composites obtained from waste tyres: a review, J. Clean. Prod. 147 (2017) 560–571, https://doi.org/10.1016/j.jclepro.2017.01.121, mars.
[3] C. Radheshkumar, J. Karger-Kocsis, Thermoplastic dynamic vulcanisates containing LDPE, rubber, and thermochemically reclaimed ground tyre rubber, Plast. Rubber Compos. 31 (3) (2002) 99–105, https://doi.org/10.1179/146580102225003074, mars.
[4] P. Lima, J. Oliveira, V. Costa, Partial replacement of EPDM by GTR in thermoplastic elastomers based on PP/EPDM: effects on morphology and mechanical properties, J. Appl. Polym. Sci. 131 (8) (2014), https://doi.org/10.1002/app.40160.
[5] O. Oguz, N. Candau, M.K. Citak, F.N. Cetin, S. Avaz Seven, Y.Z. Menceloglu, A sustainable approach to produce stiff, super-tough, and heat-resistant poly(lactic acid)-based green materials, ACS Sustain. Chem. Eng. 7 (8) (2019) 7869–7877, https://doi.org/10.1021/acssuschemeng.9b00319, avr.
[6] N. Candau, O. Oguz, N. León Albiter, G. Förster, M.L. Maspoch, Poly (lactic acid)/ground tire rubber blends using peroxide vulcanization, Polymers 13 (9) (2021), https://doi.org/10.3390/polym13091496. Art. no 9, janv.
[7] L. Asaro, M. Gratton, S. Seghar, N. Aït Hocine, Recycling of rubber wastes by devulcanization, Resour. Conserv. Recycl. 133 (2018) 250–262, https://doi.org/10.1016/j.resconrec.2018.02.016, juin.
[8] X. Zhang, C. Lu, M. Liang, Properties of natural rubber vulcanizates containing mechanochemically devulcanized ground tire rubber, J. Polym. Res. 16 (4) (2009) 411–419, https://doi.org/10.1007/s10965-008-9243-x, juill.
[9] J. Karger-Kocsis, L. Mészáros, T. Bárány, Ground tyre rubber (GTR) in thermoplastics, thermosets, and rubbers, J. Mater. Sci. 48 (1) (2013) 1–38, https://doi.org/10.1007/s10853-012-6564-2, janv.
[10] K. Fujimoto, T. Nishi, T. Okamoto, Studies on structure and physical properties of vulcanizates containing comminuted vulcanizates-6. Influence of the type of crosslinks on the physical properties of composites, Int. Polym. Sci. Technol. 8 (1981), 30.
[11] M. Tosaka, Strain-induced crystallization of crosslinked natural rubber as revealed by X-ray diffraction using synchrotron radiation, Polym. J. 39 (12) (2007), https://doi.org/10.1295/polymj.PJ2007059. Art. no 12, déc.
[12] P.-A. Albouy, P. Sotta, Strain-induced crystallization in natural rubber, in: F. Auriemma, G.C. Alfonso, C. de Rosa (Eds.), Polymer Crystallization II: from Chain Microstructure to Processing, Springer International Publishing, Cham, 2017, pp. 167–205, https://doi.org/10.1007/12_2015_328.
[13] Y. Ikeda, A. Kato, S. Kohjiya, Y. Nakajima, Rubber science and technics toward the next century: a prospective view, in: Rubber Science: A Modern Approach, Springer, Éd. Singapore, 2018, pp. 193–205, https://doi.org/10.1007/978-981-10-2938-7_6. Y. Ikeda, A. Kato, S. Kohjiya, et Y. Nakajima.
[14] B. Huneau, Strain-induced crystallization OF natural rubber: a review OF X-ray diffraction investigations, Rubber Chem. Technol. 84 (3) (2011) 425–452, https://doi.org/10.5254/1.3601131, sept.

[15] Y. Ikeda, Y. Yasuda, K. Hijikata, M. Tosaka, S. Kohjiya, Comparative study on strain-induced crystallization behavior of peroxide cross-linked and sulfur cross-linked natural rubber, Macromolecules 41 (15) (2008) 5876–5884, https://doi.org/10.1021/ma800144u, août.
[16] N. Candau, L. Chazeau, J.-M. Chenal, C. Gauthier, E. Munch, Complex dependence on the elastically active chains density of the strain induced crystallization of vulcanized natural rubbers, from low to high strain rate, Polymer 97 (2016) 158–166, https://doi.org/10.1016/j.polymer.2016.05.020, août.
[17] S. Trabelsi, P.-A. Albouy, J. Rault, Stress-induced crystallization properties of natural and synthetic CIS-polyisoprene, Rubber Chem. Technol. 77 (2) (2004) 303–316, https://doi.org/10.5254/1.3547825, mai.
[18] P.-Y. Le Gac, P.-A. Albouy, D. Petermann, Strain-induced crystallization in an unfilled polychloroprene rubber: kinetics and mechanical cycling, Polymer 142 (2018) 209–217, https://doi.org/10.1016/j.polymer.2018.03.034, avr.
[19] F. Yeh, B.S. Hsiao, B.B. Sauer, S. Michel, H.W. Siesler, In-situ studies of structure development during deformation of a segmented poly(urethane−urea) elastomer, Macromolecules 36 (6) (2003) 1940–1954, https://doi.org/10.1021/ma0214456, mars.
[20] N. Candau, et al., Mechanical reinforcement and memory effect of strain-induced soft segment crystals in thermoplastic polyurethane-urea elastomers, Polymer 223 (2021) 123708, https://doi.org/10.1016/j.polymer.2021.123708, mai.
[21] N. Candau, L. Chazeau, J.-M. Chenal, C. Gauthier, E. Munch, A comparison of the abilities of natural rubber (NR) and synthetic polyisoprene cis-1,4 rubber (IR) to crystallize under strain at high strain rates, Phys. Chem. Chem. Phys. 18 (5) (2016) 3472–3481, https://doi.org/10.1039/C5CP06383C, janv.
[22] S. Sun, Y. Lu, B.S. Hsiao, D. Wang, L. Zhang, Comprehensive study on temperature-induced crystallisation and strain-induced crystallisation behaviours of natural rubber/isoprene rubber blends, Plast. Rubber Compos. 46 (7) (2017) 290–300, https://doi.org/10.1080/14658011.2017.1335481, août.
[23] M. Wunde, M. Klüppel, Influence OF phase morphology and filler distribution IN NR/BR and NR/SBR blends ON fracture mechanical properties, Rubber Chem. Technol. 89 (4) (2016) 588–607, https://doi.org/10.5254/rct.16.83795, déc.
[24] H. Ismail, H.C. Leong, Curing characteristics and mechanical properties of natural rubber/chloroprene rubber and epoxidized natural rubber/chloroprene rubber blends, Polym. Test. 20 (5) (2001) 509–516, https://doi.org/10.1016/S0142-9418(00)00067-2, janv.
[25] B.T. Poh, G.K. Khok, Tensile property of epoxidized natural rubber/natural rubber blends, Polym. Plast. Technol. Eng. 39 (1) (2000) 151–161, https://doi.org/10.1081/PPT-100100021, févr.
[26] S. Trabelsi, P.-A. Albouy, J. Rault, Effective local deformation in stretched filled rubber 36 (24) (2003) 9093–9099, https://doi.org/10.1021/ma0303566, déc.
[27] J.-M. Chenal, C. Gauthier, L. Chazeau, L. Guy, Y. Bomal, Parameters governing strain induced crystallization in filled natural rubber, Polymer 48 (23) (2007) 6893–6901, https://doi.org/10.1016/j.polymer.2007.09.023, nov.
[28] Z.-T. Xie, et al., Effects of graphene oxide on the strain-induced crystallization and mechanical properties of natural rubber crosslinked by different vulcanization systems, Polymer 151 (2018) 279–286, https://doi.org/10.1016/j.polymer.2018.07.067, août.
[29] Y. Nie, G. Huang, L. Qu, X. Wang, G. Weng, J. Wu, New insights into thermodynamic description of strain-induced crystallization of peroxide cross-linked natural rubber filled with clay by tube model, Polymer 52 (14) (2011) 3234–3242, https://doi.org/10.1016/j.polymer.2011.05.004, juin.
[30] S.Z. Salleh, M.Z. Ahmad, H. Ismail, Properties of natural rubber/recycled chloroprene rubber blend: effects of blend ratio and matrix, Procedia Chem. 19 (2016) 346–350, https://doi.org/10.1016/j.proche.2016.03.022, janv.
[31] G. Mathew, R.P. Singh, N.R. Nair, S. Thomas, Recycling of natural rubber latex waste and its interaction in epoxidised natural rubber, Polymer 42 (5) (2001) 2137–2165, https://doi.org/10.1016/S0032-3861(00)00492-4, mars.
[32] H.S. Ahmad, H. Ismail, A.R. Azura, Comparison properties of natural rubber/virgin acrylonitrile–butadiene rubber and natural rubber/recycled acrylonitrile–butadiene rubber blends, Iran. Polym. J. (Engl. Ed.) 24 (3) (2015) 185–195, https://doi.org/10.1007/s13726-015-0310-y, mars.
[33] H. Nabil, H. Ismail, A.R. Azura, Compounding, mechanical and morphological properties of carbon-black-filled natural rubber/recycled ethylene-propylene-diene-monomer (NR/R-EPDM) blends, Polym. Test. 32 (2) (2013) 385–393, https://doi.org/10.1016/j.polymertesting.2012.11.003, avr.
[34] J. Kruželák, R. Sýkora, I. Hudec, Peroxide vulcanization of natural rubber. Part I: effect of temperature and peroxide concentration, J. Polym. Eng. 34 (7) (2014) 617–624, https://doi.org/10.1515/polyeng-2014-0034, sept.
[35] P.J. Flory, J. Rehner, Statistial mechanics of cross-linked polymer networks II. Swelling. textitJ, Chem. Phys. 11 (1943) 521–526.
[36] R. Joseph, K.E. George, D.J. Francls, K.T. Thomas, Polymer-solvent interaction parameter for NR/SBR and NR/BR blends, Int. J. Polym. Mater. Polym. Biomater. 12 (1) (1987) 29–34, https://doi.org/10.1080/00914038708033918, nov.
[37] G. Kraus, Swelling of filler-reinforced vulcanizates, J. Appl. Polym. Sci. 7 (3) (1963) 861–871, https://doi.org/10.1002/app.1963.070070306.
[38] N. Candau, O. Oguz, E. Peuvrel-Disdier, J.-L. Bouvard, C. Pradille, , et al.N. Billon, Strain-induced network chains damage in carbon black filled EPDM, Polymer 175 (2019) 329–338, https://doi.org/10.1016/j.polymer.2019.05.017, juin.
[39] N. Candau, O. Oguz, E. Peuvrel-Disdier, J.-L. Bouvard, C. Pradille, , et al.N. Billon, Strain and filler ratio transitions from chains network to filler network damage in EPDM during single and cyclic loadings, Polymer 197 (2020) 122435, https://doi.org/10.1016/j.polymer.2020.122435, mai.
[40] C.E. Federico, G. Rauchs, O. Kotecky, S. Westermann, F. Addiego, Cavitation in thermoplastic-reinforced rubber composites upon cyclic testing: multiscale characterization and modelling, Polymer 211 (2020) 123084, https://doi.org/10.1016/j.polymer.2020.123084, déc.
[41] H.M. James, E. Guth, Theory of the elastic properties of rubber, J. Chem. Phys. 11 (10) (1943) 455–481, https://doi.org/10.1063/1.1723785, oct.
[42] L.R.G. Treloar, The Physics of Rubber Elasticity, Oxford University Press, USA, 1975.
[43] A. Kloczkowski, M.A. Sharaf, J.E. Mark, Computer simulations on filled elastomeric materials, Chem. Eng. Sci. 49 (17) (1994) 2889–2897, https://doi.org/10.1016/0009-2509(94)E0107-2, sept.
[44] J.E. Mark, Rubber elasticity, J. Chem. Educ. 58 (11) (1981) 898, https://doi.org/10.1021/ed058p898, nov.
[45] J. Araujo-Morera, R. Verdugo-Manzanares, S. González, R. Verdejo, M.A. Lopez-Manchado, M. Hernández Santana, On the use of mechano-chemically modified ground tire rubber (GTR) as recycled and sustainable filler in styrene-butadiene rubber (SBR) composites, J. Compos. Sci. 5 (3) (2021), https://doi.org/10.3390/jcs5030068. Art. no 3, mars.
[46] N. Candau, et al., Strain-induced crystallization of natural rubber and cross-link densities heterogeneities, Macromolecules 47 (16) (2014) 5815–5824, https://doi.org/10.1021/ma5006843, août.
[47] J.-B. Le Cam, E. Toussaint, Volume variation in stretched natural rubber: competition between cavitation and stress-induced crystallization, Macromolecules 41 (20) (2008) 7579–7583, https://doi.org/10.1021/ma801290w, oct.
[48] Y. Merckel, J. Diani, M. Brieu, J. Caillard, Effects of the amount of fillers and of the crosslink density on the mechanical behavior of carbon-black filled styrene butadiene rubbers, J. Appl. Polym. Sci. 129 (4) (2013) 2086–2091, https://doi.org/10.1002/app.38925.
[49] N. Candau, et al., Heat source and voiding signatures of Mullins damage in filled EPDM, Polym. Test. 91 (2020) 106838, https://doi.org/10.1016/j.polymertesting.2020.106838, nov.
[50] E. Guth, Theory of filler reinforcement, Rubber Chem. Technol. 18 (3) (1945) 596–604, https://doi.org/10.5254/1.3546754, sept.
[51] P.J. Flory, Thermodynamics of crystallization in high polymers. I. Crystallization induced by stretching, J. Chem. Phys. 15 (6) (1947) 397–408, https://doi.org/10.1063/1.1746537, juin.
[52] Y. Fukahori, Mechanism of the self-reinforcement of cross-linked NR generated through the strain-induced crystallization, Polymer 51 (7) (2010) 1621–1631, https://doi.org/10.1016/j.polymer.2010.01.059, mars.
[53] S. Poompradub, et al., Mechanism of strain-induced crystallization in filled and unfilled natural rubber vulcanizates, J. Appl. Phys. 97 (10) (2005) 103529, https://doi.org/10.1063/1.1900927, mai.
[54] C.W. Bunn, W.H. Bragg, Molecular structure and rubber-like elasticity I. The crystal structures of β gutta-percha, rubber and polychloroprene, Proc. R. Soc. Lond. Ser. Math. Phys. Sci. 180 (980) (1942) 40–66, https://doi.org/10.1098/rspa.1942.0024, mars.
[55] N. Candau, L. Chazeau, J.-M. Chenal, C. Gauthier, E. Munch, Compared abilities of filled and unfilled natural rubbers to crystallize in a large strain rate domain, Compos. Sci. Technol. 108 (2015) 9–15, https://doi.org/10.1016/j.compscitech.2014.12.014, févr.
[56] J.-B. Le Cam, P.-A. Albouy, S. Charlès, Comparison between x-ray diffraction and quantitative surface calorimetry based on infrared thermography to evaluate strain-induced crystallinity in natural rubber, Rev. Sci. Instrum. 91 (4) (2020), 044902, https://doi.org/10.1063/1.5141851 avr.